Application of CT Simulation Technique for Virtual Fecal Tagging in CTC

Zepa Yang[1], Hyeong-min Jin[3,4], and Jong Hyo Kim[2,3,4,5]

[1] Department of Biomedical Sciences
[2] Department of Radiology
[3] Interdisciplinary Program in Radiation Applied Life Science,
Seoul National University College of Medicine
[4] Institute of Radiation Medicine, Seoul National University Medical Research Center,
101 Daehangno, Jongno-gu, Seoul 110-744, Korea
{yangzepa,hmjin,kimjhyo}@snu.ac.kr
[5] Department of Intelligent Convergence Systems,
Graduate School of Convergence Science and Technology, Seoul National University,
864-1, Iui-dong, Yeongtong-gu, Suwon-si, Gyeonggi-do 443-270, Korea

Abstract. An integrative CT simulation technique is presented that creates realistic CT images of virtual fecal-tagged material that was added to given clinical DICOM CT images. The energy spectrum of the CT X-ray source, the energy-dependent attenuation, and the scattering properties of the soft tissue and tagging material were incorporated in the generation technique for the DICOM image-based virtual sinograms, followed by CT reconstruction reflecting the vendor-specific filtering kernels. Dark band artifacts were generated by appropriate combining of beam-hardening and -scattering effects into the generation procedure for the virtual sinograms. We used a set of simple numerical phantoms to assess the basic behavior of artifact production. A reference set of CTC images with and without tagging material and artifacts was used for evaluation of the realism of the simulated results. The level of realism was evaluated in terms of the artifact strength and patterns around the added tagging material, compared to real tagging images. The results showed that our CT simulation technique provides sufficient realism for virtual fecal-tagged images that reflect a chain of physical and numerical processes, including beam hardening, scattering, and vendor-specific kernel filtered backprojection. The technique presented has the potential to be used as a tool for investigating the effect of tagging materials on image quality and to gauge how well the electronic cleansing technique performs.

Keywords: CT simulation, virtual tagging, CTC, artifact, beam hardening, scattering effect.

1 Introduction

CT colonography is a promising method in colon cancer screening, which provides a sensitivity comparable to that of optical colonoscopy for detecting polyps 10 mm and

H. Yoshida, D. Hawkes, M.W. Vannier (Eds.): Abdominal Imaging 2012, LNCS 7601, pp. 58–68, 2012.

larger [1]. Its ability to examine the whole-colon structure non-invasively in a time-efficient manner, without needing sedation and recovery time, places CTC as an attractive alternative to optical colonoscopy in the screening and surveillance steps of colon cancer diagnosis [1].

In an effort to reduce the patient's burden of the full cathartic bowel preparation currently required for CTC examination, studies are being carried out for the development of a noncathartic or a less intense cathartic bowel preparation in combination with an electronic bowel-cleansing technique [2]. In the research pathways towards optimizing the bowel preparation technique, a combination of studies would be needed before the final conclusion is reached, which would require huge costs and efforts, especially when varying image qualities with different tagging regimens are compared. Because tagging regimens with different materials and concentrations could generate varying degrees of artifacts in CT examinations, the performance of the visual examination as well as the electronic cleansing technique could be impaired depending on the resulting image quality due to the specific tagging regimen applied to the study. In addition, the image quality and the artifacts generated in CT are related to the patient's body structure in a complex manner; the same tagging regimen would generate different artifacts in different patients. Ideally, different tagging regimens should be applied to the same patients so that one can objectively compare the image quality and artifacts resulting from each specific tagging regimen; however, it is practically and ethically impossible.

The motivation for this study was to develop a technique that allows for virtual tagging on CTC images with different combinations of tagging materials and concentrations. This technique was applied to a CT simulation technique that included the energy-dependent attenuation characteristics of the tagging materials and of the body. We calculated the beam hardening and scattering process along the beam path within the body, which resulted in a realistic virtual tagging image with artifacts generated by the complex interactions of the tagging material with the X-ray energy and the body of the patient.

We describe the basic physical principle involved in beam hardening and scatter generation, present a simple experiment with numerical phantoms, and discuss the preliminary results in terms of clinical CTC cases.

2 Materials and Methods

2.1 Numerical Phantoms

A set of numerical phantoms that contained an oval-shaped disk of water and a circular disk of calcium was created, representing the human body and the spine, respectively, and multiple holes with air representing the insufflated colon. A hole was filled with iodine to varying levels of depths and concentrations to mimic the fecal tagging material. The numerical phantoms were used for assessment of the proper CT simulation technique.

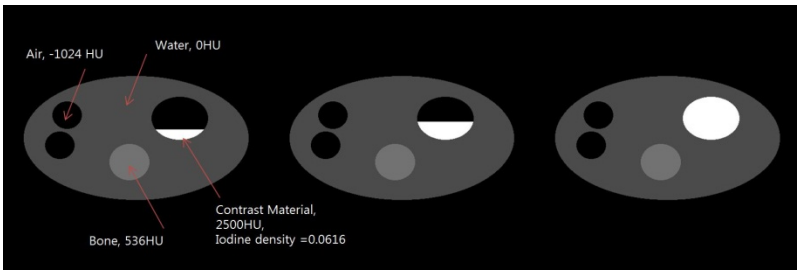

Fig. 1. Numerical phantom dataset. The intensities of each phantom are based on the parts of the CT images and contrast material and are based also on the iodine-based tagging regimen (OMNIPAQUE 300 mg/mL) and the density for the ratio in the clinical case. The window level of the image was changed to the best view of the HU value for each component.

2.2 Clinical Dataset

Selected CTC images were used from the CTC case database at the Seoul National University Hospital. CT examinations were performed with an MDCT (Siemens SOMATOM Definition, Philips Brilliance 64) under low-dose conditions (120 kVp, 40 ~ 55 mAs) and an iodine-based tagging regimen (OMNIPAQUE, 300mg/mL, Nycomed) was applied in the CTC cases used in this study.

We used DICOM images containing tagging material in the colon and exhibiting beam-hardening artifacts in the colon as a reference dataset to evaluate the degree of artifacts depending on the tagging concentration and the body configuration.

Fig. 2 shows sample reference images and line profiles revealing the degree of the dark-band artifacts around the tagging material. Table 1 summarizes the measured CT values at the tagging material and at a location with the most severe darkening artifact. As is shown, the degree of the artifacts has a complex relationship with the geometric configuration and concentration of the tagging material and with the body shape and the relative distance and location of another highly attenuating structure.

A separate set of DICOM images was collected which do not show tagging material or artifacts at a given slice, to be used as a substrate for addition of virtual-tagging material and for evaluation of the virtual-tagging effect.

Fig. 2. Various CT images with artifacts that lowered the tissue intensity

Table 1. Intensity of the contrast agent in the images with artifacts; the distorted intensity of the tissues compared to the normal tissues around the artifacts; the size of the contrast material; and the percent of contrast filling in the colon area. Distorted values are dependent on the contrast intensity of its source, its location, and the tissue material.

Intensity of the tagging material (HU)	Tissue intensity distortion (HU)	Length of the contrast material (mm)	Colon filling (%)
1186	-214	21 mm	13%
1787	-498	35 mm	33%
1579	-520	42 mm	21%
895	-115	24 mm	35%
1180	-211	16 mm	8%
1170	-282	27 mm	17%
972	-208	31 mm	30%
1050	-440	52 mm	25%

2.3 Simulation of X-Ray Interaction with Matter

2.3.1 CT Simulation

For a simple fan-beam CT simulation, an in-house CT projection/backprojection tool was created. The simulation software code was created with MFC (Microsoft Visual Studio was used). The basic algorithm for the projection/backprojection was based on the following equations:

$$P_\gamma(\xi) = \int_0^s \mu\big(\xi(x,y), \eta(x,y)\big) d\eta, \tag{1}$$

$$\mathrm{g(x,y)} = \int_0^\pi P_\gamma(\xi) d\,\gamma, \tag{2}$$

where P_γ is the projection data (sinogram), μ is the original CT image, ξ the projection angle, η the count of projection rays, and g the backprojected image [3].

2.3.2 Beam Hardening Simulation

During the process of penetration through an object, the energy profile of a polychromatic X-ray beam changes continuously at each step of attenuation along the path. This is because different bands of the energy spectrum attenuate differently depending on the specific attenuation coefficient of the material being imaged. In general, low-energy radiation, such as soft X-ray beams, is more strongly absorbed than high-energy radiation, such as hard X-ray beams [3]. This beam-hardening effect is a major source of dark-band artifacts seen on CT images that contain contrast agents.

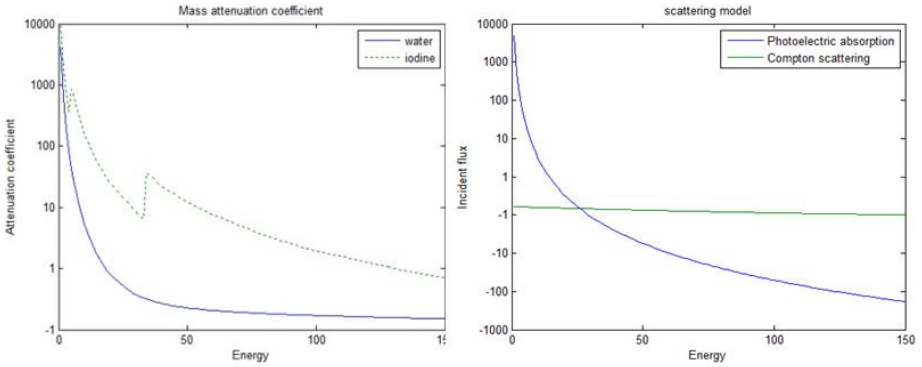

Fig. 3. A) Scattering model for total transmission, photoelectric absorption, and Compton scattering. B) Mass attenuation coefficients of water and iodine. These values were obtained from the National Institute of Standards and Technology (NIST) website.

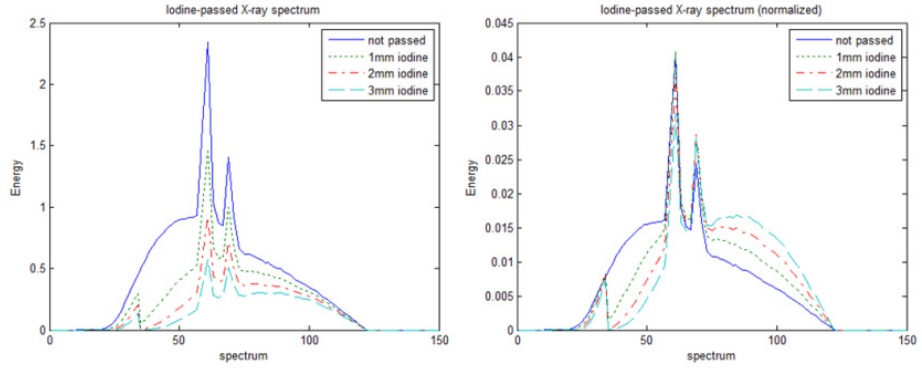

Fig. 4. A) Various thicknesses of iodine-passed X-ray characteristic spectrum and B) the normalized spectrum. A beam-hardening effect can be seen in the normalized spectrum; the low-energy part is degraded and the high-energy part is enhanced. The base X-ray characteristic spectrum was simulated with the tungsten anode spectral model by use of TASMIP, with 120 keV and a 3 mm aluminum filter.

Equation (3) describes the basic principle of X-ray attenuation used in this study for calculation of the beam-hardening process:

$$I_t(E) = \int I_0(E) e^{-\int \frac{\mu(E)}{\rho} x \, dx} dE, \tag{3}$$

where $\mu(E)$ is the energy-dependent mass attenuation coefficient, ρ is the density, and x is the thickness of the material that the x-ray spectrum has transmitted [3].

The X-ray spectrum was obtained from a published model for a tungsten anode spectral model by use of interpolating polynomials (TASMIP), with the application of 120 KVp and a 3 mm aluminum filter [4]. Beam hardening was calculated only for the iodine material, and the attenuation coefficient of water after passing the iodine material was updated by application of the hardened beam profiles to the spectral attenuation coefficients of water, as shown in Fig. 4.

X-ray attenuation is due to photoelectric absorption, Compton scattering, and Rayleigh scattering. The total spectral attenuation coefficient μ_{Total} is given by

$$\mu_{Total} = \mu_{photo} + \mu_{Compton} + \mu_{Rayleigh}, \tag{4}$$

$$\mu_{Photo} = \mathrm{k}\frac{\rho}{A}\frac{Z^4}{h\nu^3}, \tag{5}$$

$$\mu_{Compton} = n \cdot 2\pi r_e^2 \left[\left(\frac{1+\varepsilon}{\varepsilon^2}\right)\left(2\frac{1+\varepsilon}{1+2\varepsilon^2} + \frac{\ln(1+2\varepsilon)}{\varepsilon}\right) + \frac{\ln(1+2\varepsilon)}{2\varepsilon} - \frac{1+3\varepsilon}{(1+2\varepsilon)^2}\right]. \tag{6}$$

For an analytical approximation, $\mu_{Rayleigh}$ was regarded as having a small, negligible contribution [5].

The values for the mass attenuation coefficients of iodine, water, aluminum, etc. were obtained from a publicly available database [7].

2.3.3 Scattering Simulation

Besides beam hardening, scattering is another important source of X-ray interaction with matter, which contributes strongly to the dark-band artifacts seen in CTC studies containing tagging materials. Although the Monte Carlo simulation technique is frequently used for calculation of the scattering process, it is impractically slow for use in CT simulation, which requires creating thousands of projection images per single CT image. Instead, we used a simple iterative-convolution model at each step of the ray path. The primary and the scattered transmission in water were calculated by use of the following equations:

$$T_p = \frac{I_{t(x)}}{I_o} = \int S(E) e^{-\int \mu_{photo}(total,E(\eta))x d\eta} dE, \tag{7}$$

$$T_s = \mathrm{G} \circledast \int S(E) e^{-\int \mu_{Compton}(water,E(\eta))x d\eta}\, dE, \tag{8}$$

where G is the Gaussian filter convolution, x the thickness, and S(E) is the weighting function derived by the following equation:

$$\mathrm{S(E)} = \frac{I_o(E)}{\int I_o\,(E)}. \tag{9}$$

The relative fraction of the photoelectric absorption and the Compton scattering of water were used as weighting factors of the primary and scattered transmission for obtaining the total transmission at a given ray step:

$$T_t = T_p + k\,T_s, \tag{10}$$

where k is the scattering-factor constant.

After calculating the total transmission, we converted the value to a sinogram for the backprojection process.

Because the CT images are already filtered on the vendor-specific filtered backprojection process of their creation, if the images are projected and backprojected again, the images may have changes in the intensity and structure (i.e. blurring or over-sharpening by various filters). To avoid this, we acquired a sinogram from the original CT image, and we subtracted it from the sinogram of the virtual ray projection to yield a sinogram that only had the information for the beam-hardening effects and scattering artifacts. We backprojected the subtracted sinogram to acquire the image for the artifact part and finally added to the original CT image to get the artifact-simulated fecal-tagged image.

2.3.4 Integrated CT Simulation

To create realistic CT images containing tagging materials and artifacts, we applied an integrated CT simulation technique including image-based material decomposition, virtual sinogram projection, beam hardening and scatter simulation, and vendor-specific kernel filtering. Fig. 5 shows the overall procedure of our integrated CT simulation procedure.

In the image preparation step, the CT image of interest was used as a substrate; a tagging-component image was created by application of the attenuation coefficient and concentration of the tagging material; a water-component image was created by application of a threshold to the substrate image and adding the water part of the tagging-component image. Finally, a component sum image was created by addition of the tagging component image to the substrate image.

In the virtual-sinogram projection step, the ray projection was applied to the tagging component, water component, and component sub-images for calculation of the beam hardening, scattering, and photoelectric effects during ray penetration.

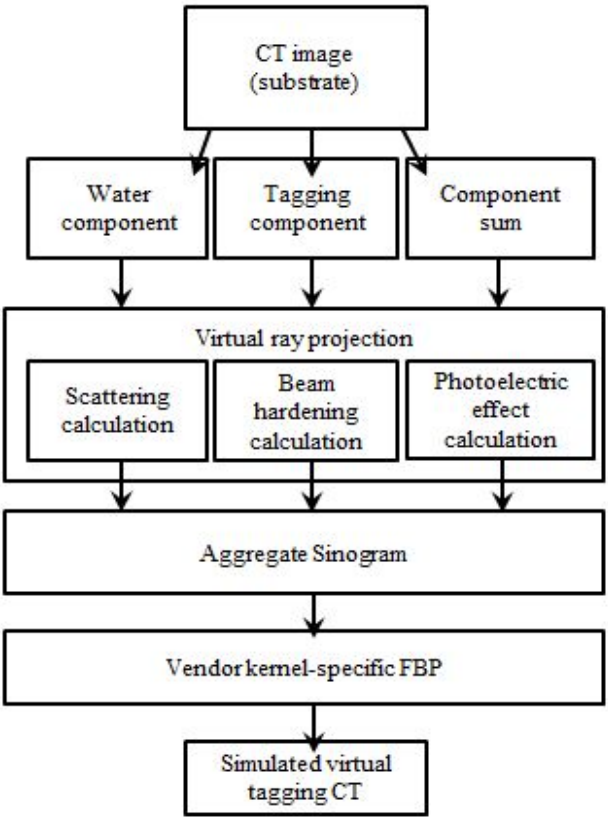

Fig. 5. Process box flowchart of the proposed method for simulating virtual fecal-tagged images

After the ray projection was completed, each component projection was weighted and added to create an aggregate sinogram, followed by vendor-specific kernel filtering, and finally backprojected to create the simulated CT of the virtual-tagging data.

3 Results

The initial simulation was tested with the numerical phantoms at various densities. Fig. 6 shows oval phantoms with various iodine fill levels and densities. The intensity and size of the artifacts varied depending on the density and the percent of iodine filling.

From the results of the evaluation, we found that the pattern of streak artifacts and their tissue intensity distortion were almost similar. In clinical trials, realistic CT images with artifacts were simulated successfully.

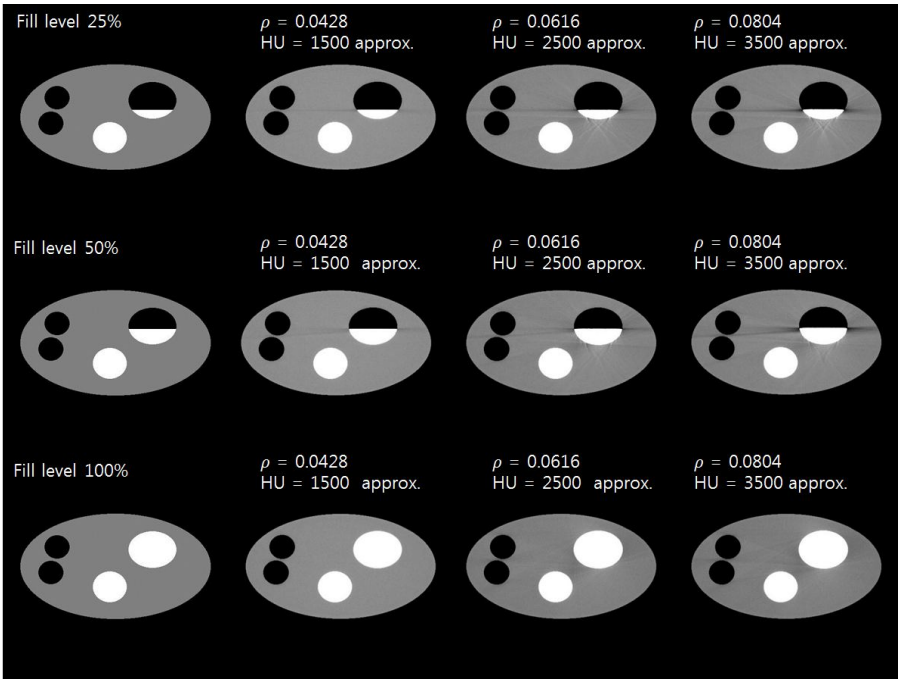

Fig. 6. Simulation results for the numerical phantoms with varying levels of colon filling and iodine density. The level of streak artifact varies depending on both iodine density and level of filling. The window width and the level of the image were adjusted to yield the best view of the artifacts.

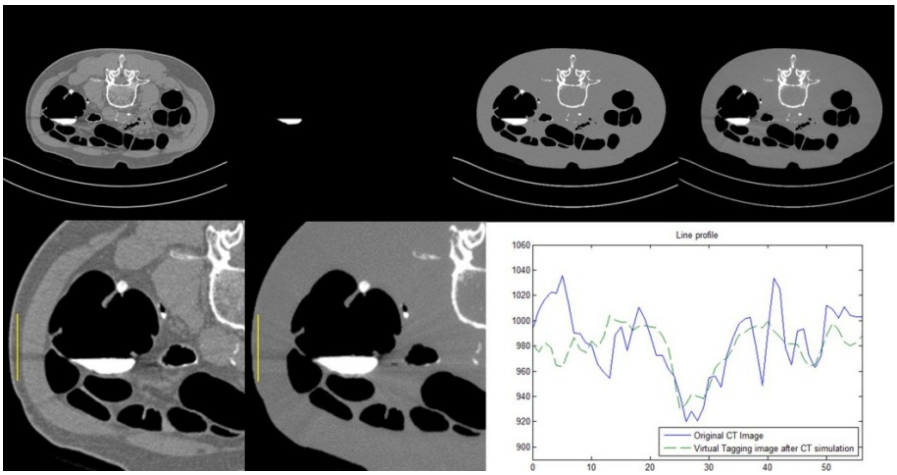

Fig. 7. A) CT image with artifacts, B) iodine mask, C) tissue normalized results with iodine mask, D) simulated result, and E) line profile of the original CT image and the virtual- tagging CT image result. Distorted values and their patterns are almost similar.

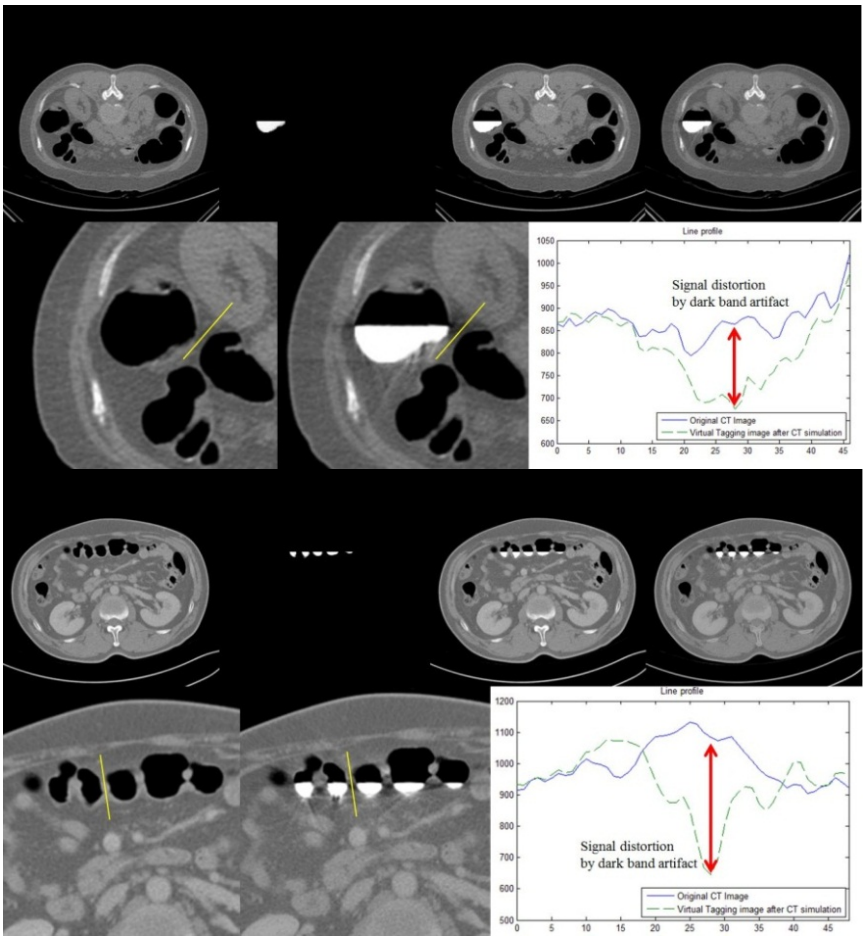

Fig. 8. A) Original CT images without artifacts, B) iodine-targeted image, C) iodine-mask added image, and D) CT simulated virtual fecal-tagged CT images. Beam-hardening and scattering artifacts were successfully generated. B) Line profile of the original CT image and virtual tagged image.

4 Conclusion

By use of the process described, virtual fecal-tagged CTC images can be generated at any location and for any circumstance. This result could contribute to the collection and practical use of patient data for research. Furthermore, it can be used as concrete datasets for CT colonography research in the future.

5 Discussion

This study presented an integrative CT simulation technique which could produce realistic dark-band artifacts caused by highly attenuating fecal tagging agents in CTC

studies. Dark-band artifacts are frequently seen in CTC studies with fecal tagging, and then often cause problems in electronic cleansing and polyp detection procedures in CAD systems. As shown in Table 1, the intensity of dark bands appears to be associated with several factors, including the density of the tagging agent, the level of fluid filling the colon, the width of filling, and the size of body. Although CT systems apply sophisticated techniques in the reconstruction procedure to reduce the dark-band artifacts, these artifacts still remain as a challenging problem not yet overcome.

Our study elucidated the physical process behind the generation of the dark-band artifacts. Whereas the these artifacts are usually called beam-'hardening artifacts', our study showed that these artifacts are, in fact, generated by a combination of beam-hardening and scattering effects which are two fundamental processes of x-ray interaction with matter. In this study, we did not attempt to apply the proposed technique to removal of the dark-band artifacts. Although our simulation technique has such a potential, artifact removal would involve additional steps of specialized techniques which remain a subject for further study.

In its current form, however, the presented technique could be used in the evaluation of electronic cleansing techniques and polyp detection techniques in CTC under the fecal-tagging condition by providing an artifact-free image as the ground truth as well as the simulated virtual fecal-tagging image with dark-band artifacts as test data. This study is limited in that only fluid-state tagging material was considered. As various tagging regimens are being tried clinically, extending the tagging models of our simulation framework to include materials of solid or semi-solid forms which may appear as particles or thin surface layers would be necessary for advancement of this study to a more practical level.

References

1. McFarland, E.G., Levin, B., Lieverman, D.A., Pickhardt, P.J., Johnson, C.D., Glick, S.N., Brooks, D., Smith, R.A.: American Cancer Society, U.S. Multisociety Task Force on Colorectal Cancer, American College of Radiology: Revised Colorectal Screening Guidelines: Joint Effect of the American Cancer Society, U.S. Multisociety Task Force on Colorectal Cancer, and American College of Radiology. Radiology 248, 717–720 (2008)
2. Cai, W., Zalis, M.E., Näppi, J., Harris, G.J., Yoshida, H.: Structure-Analysis Method for Electronic Cleansing in Cathartic and Noncathartic CT Colonography. Med. Phys. 35, 3259–3277 (2008)
3. Buzug, T.M.: Computed Tomography: From Photon Statistics to Modern Cone-Beam CT. Springer, Heidelberg (2008)
4. Boone, J.M., Fewell, T.R., Jennings, R.J.: Molybdenum, Rhodium, and Tungsten Anode Spectral Models Using Interpolating Polynomials with Application to Mammography. Med. Phys. 24, 1863–1874 (1997)
5. Heismann, B.J., Leppert, J., Stierstorfer, K.: Density and Atomic Number Measurements with Spectral X-Ray Attenuation Method. J. Appl. Phys. 94, 2073–2079 (2003)
6. Ruhrnschopf, E.P., Klingenbeck, K.: A General Framework and Review of Scatter Correction Methods in Cone Beam CT. Part 2: Scatter Estimation Approaches. Med. Phys. 38, 5186–5199 (2011)
7. Hubbell, J.H., Seltzer, S.M.: Tables of X-Ray Mass Attenuation Coefficients and Mass Energy-Absorption Coefficients from 1 keV to 20 MeV for Elements Z=1 to 92 and 48 Additional Substances of Dosimetric Interest*, http://www.nist.gov/pml/data/xraycoef/index.cfm